ECTI Transactions on Computer and Information Technology
Journal homepage: https://ph01.tci-thaijo.org/index.php/ecticit/
Published by the ECTI Association, Thailand, ISSN: 2286-9131

Plaque Territory Detection in IVUS Images based on Concentration of Entropy and Gradient Magnitude via Spiral Random Walk-based Approach

Benchaporn Jantarakongkul[1] and Pusit Kulkasem[2]

ABSTRACT

This paper presents a simple and optimal approach for automatically identifying the location and size of plaque territories in IVUS images, thus improving plaque territory classification. Unlike existing circular-based algorithms, we leverage the anatomical structure of IVUS images to enhance accuracy. The adventitia, which constitutes the largest part of the image, serves as a landmark; however, its low contrast makes edge detection challenging. To address this issue, we enhance the brightness of the adventitia, identify and remove intima blobs, and accurately determine the media boundary. This aids in simplifying the calculation of plaque territory. To locate the plaque territory, we employ a spiral random walk-based approach that utilizes the concentration of entropy and gradient magnitude in the target area. Our approach outperforms existing methods, contributing to automated plaque analysis for cardiovascular disease diagnosis and treatment. The results show that the proposed approach achieves an accuracy of 0.89, precision of 0.81, recall of 0.77, and F1-Score of 0.83, respectively.

Article information:

Keywords: Plaque Territory Classification, IVUS Images, Brightness Enhancement, Blob Analysis, Region of Interest (ROI), Cardiovascular Diseases

Article history:
Received: September 8, 2023
Revised: September 17, 2023
Accepted: September 21, 2023
Published: September 23, 2023 (Online)

DOI: 10.37936/ecti-cit.2023173.253328

1. INTRODUCTION

Arterial plaque is a leading contributor to heart disease. If not addressed, it can precipitate heart attacks and other life-threatening conditions. Blood vessels, which are responsible for promoting blood flow and supplying oxygen to the heart and other tissues, play a critical role in sustaining life. However, untreated coronary artery disease, triggered by the accumulation of calcium or fatty deposits on arterial walls, can result in heart failure or other life-threatening conditions.

In recent years, intravascular ultrasound (IVUS) technology has emerged as an instrumental tool for detecting and analyzing calcium and fatty deposits in coronary arteries. IVUS images afford high-resolution cross-sectional views of the coronary artery wall, enabling accurate detection of fatty and calcified plaques. By gauging the size and distribution of these plaques, IVUS imaging can aid in predicting heart attacks and strokes.

The implementation of IVUS technology has significantly enhanced the accuracy and efficiency of plaque analysis through the development of automated plaque detection and quantification algorithms. This has reduced the time required for manual measurements, and decreased variability. However, a key challenge lies in the low visual contrast of IVUS images, which hampers the identification of lumen and media areas and could lead to erroneous results.

Recently, research has been conducted to investigate this issue, leading to the proposal of various solutions. For example, IVUS-Net, developed by Ji Yang et al. [1], accurately segments the lumen and media areas of human arteries in IVUS images using an FCN architecture and contour extraction, all within a mere 0.15 seconds per frame. Juhwan Lee et al. [2] utilized a deep belief network to classify dense calcium tissues in grayscale intravascular ultrasound images. In another study, Lucas Lo et al. [3] put forth a decoupled method for automatic IVUS blood vessel segmentation using Support Vector Machines (SVMs) and Random Forest (RF) for pixel classification and morphological feature recognition. Janya Onpans et al. [4] proposed an approach to segment

[1,2] The authors are with the Faculty of Informatics, Burapha University, Thailand., E-mail: benchaporn@informatics.buu.ac.th and pusit@informatics.buu.ac.th
[2] Corresponding author: pusit@informatics.buu.ac.th

the components of intravascular ultrasound (IVUS) images using ensemble Gabor-spatial features and a support vector machine (SVM) classification model. The proposed approach achieved promising results regarding the Jaccard Index, Hausdorff Distance, and Percentage Area Difference for segmenting the components of IVUS images. The classification model also demonstrated high accuracy, precision, and recall in identifying the components of IVUS images. However, the results from segmentation require further edge refinement methods to enhance the performance of the mentioned evaluation metrics. It is important to note that the proposed method only segments the IVUS's components consisting of lumen, media, and adventitia. Other components, such as plaque, are not segmented. Simone Balocco et al. [5] introduced a standardized evaluation methodology and reference database for evaluating IVUS image segmentation algorithms. The study assessed eight algorithms using this framework. Among them, four were fully automatic, and the other four were semi-automatic, requiring manual initialization by an expert. The evaluation results showed that several methods for lumen segmentation were as accurate as inter-observer variability. However, media segmentation posed more challenges. Lumen segmentation errors were mainly influenced by the presence of catheter shadow, stent, and similarity with soft plaque texture. For media segmentation, calcium and catheter shadow were major obstacles. The study identified limitations of the evaluated methods: semi-automatic algorithms showed potential for better performance but required manual interaction, while 3D algorithms exhibited greater robustness but might need more processing memory. A supervised approach based on classification required less tuning and facilitated generalization to different datasets, yet creating a training set could be time-consuming. Xinze Li et al. [6] suggested employing a multi-stage deep classifier cascade to classify coronary plaque from grayscale IVUS images. Their framework comprises one segmentation module and four classification modules, which are trained and evaluated successively. The pre-segmentation module aims to delineate potential plaque territories, and a multi-level classification strategy has been designed based on plaque histological composition and morphology. The effectiveness of these multi-stage classifiers is evaluated using IVUS images labeled by clinical cardiologists.

Based on the literature reviews, researchers have utilized a variety of techniques to address the challenges associated with low visual contrast in Intravascular Ultrasound (IVUS) images. Among these approaches, deep learning has gained significant popularity due to its ability to achieve high performance and accuracy by automatically extracting important features and producing accurate results [9][10][11]. However, it may involve higher complexity compared to traditional machine learning methods, where researchers are required to extract relevant features prior to performing classification.

In this paper, the aim of this study is to introduce a fundamental research approach that offers simplicity and optimality for segmenting the constituents of IVUS images, encompassing lumen, media, and adventitia, while simultaneously identifying attributes relevant to plaque territory classification. We employed an integrated approach that involved techniques ranging from contrast adjustment to the concentration of entropy and gradient magnitude via a spiral random walk-based approach, in order to identify plaque territory in the target area. This method automatically detects the location and size of the plaque, with a lower problem-solving complexity than deep learning methods. It differs from existing techniques, which often use circular-like algorithms like the Hough transform, Level-set methods, or k-means algorithms to detect circular structures in the media.

2. PROBLEM ANALYSIS

The anatomical structure of an IVUS image is depicted in Figure 1. From the outside in, the structure comprises four parts: the adventitia, media, intima, and lumen. We observe that the adventitia is the largest and thickest part of the input image, which can serve as an image landmark. Moreover, while the adventitia reflects the most light compared to the other parts, its reflection remains low contrast in relation to the media, intima, and lumen.

Due to this low contrast in IVUS images, which results in unclear edges that may necessitate additional time or computing resources to resolve, we have made significant strides in this paper to accurately calculate plaque territory. We propose that enhancing the brightness of the adventitia can aid in detecting the other components of the IVUS image. After this enhancement, the adventitia part is not only brighter but also contains some blobs in the intima part. Therefore, a blob analysis technique must be deployed to detect and remove these blobs. As a result, the real boundary of the media will be detected, which can be used to identify the region of interest (ROI) when calculating the plaque territory.

In summary, the intriguing research problem addressed in this paper encompasses three components:

1. Applying the Gamma Correction technique to enhance image quality. By utilizing different gamma levels for adjustments in gamma up or gamma down, we can focus on specific regions of interest. For example, in cases where our interest lies in the media, applying gamma up adjustments enables us to effectively eliminate the intervening region between the media and lumen, as illustrated in Figure 2.C or Figure 2.D. It is worth noting that the threshold values in Figure 2 are determined based on the

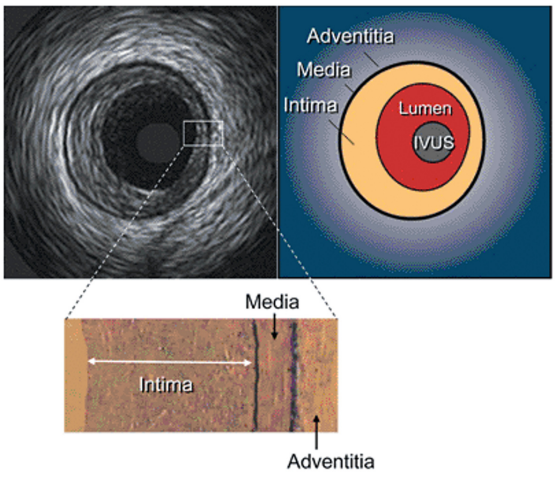

Fig.1: *Anatomy of IVUS image.*

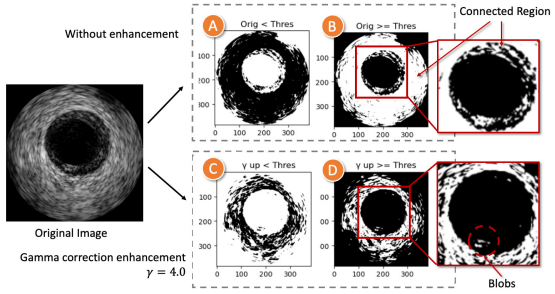

Fig.2: *Formulation of the research problem.*

histogram of brightness values from the IVUS image.

2. Calculating the boundary of the media part based on the brightness of the adventitia. This step also requires a blob analysis technique to detect and remove blobs.
3. Calculating the size and position of the plaque in the image.

Firstly, image normalization is employed to adjust the brightness levels and reduce the variation in light intensity values within the image. This step aims to ensure consistent illumination across different images, allowing for more reliable and accurate analysis and processing. By normalizing the brightness, the method mitigates the potential impact of uneven lighting conditions that could distort or obscure important image features.

Secondly, image enhancement and blob analysis techniques are utilized to further improve the visibility of the media boundary. By applying appropriate image enhancement algorithms, the method enhances the details of the media/adventitia boundary regions, enabling more precise identification and analysis. Blob analysis helps in detecting and characterizing distinct regions in the image, which contributes to better contour results.

The method also involves media boundary estimation, which is crucial for accurately identifying the boundaries of the media layer. By estimating the media boundaries, the method can precisely localize the plaque within the arterial wall. This information is then utilized in subsequent steps for more accurate plaque detection and quantification.

Additionally, the spiral random walk technique is employed to systematically explore the IVUS image and estimate the contaminated area within the media layer. This approach allows for a comprehensive analysis of the plaque distribution within the artery, enabling clinicians to visualize the accumulation of plaque in different quadrants of the media layer. This information is vital for making rapid medical decisions and developing effective treatment plans.

By incorporating these steps, the proposed method addresses the challenges associated with low visual contrast in IVUS images. It streamlines the analysis process, reduces computational complexity, and provides clinicians with a valuable tool for efficiently assessing plaque accumulation. This improved efficiency and accuracy support timely medical interventions and ultimately contribute to better patient outcomes in the diagnosis and treatment of coronary artery disease.

3. MATERIALS AND METHODS

A. Intravascular Ultrasound Image

Intravascular ultrasound (IVUS) is a medical imaging technique used to visualize the inside of coronary arteries. The cross-sectional images produced by IVUS can be mathematically represented as a stack of circular layers, with each layer representing a different depth within the artery. The thickness of each layer is determined by the transducer frequency and the speed of sound in the tissue.

Figure 1. shows the components of an IVUS image, which include the lumen, intima, media, and adventitia. The lumen refers to the innermost layer of the vessel, where blood flows. The intima is the layer that lines the lumen and is composed of endothelial cells and connective tissue. The media is the middle layer and consists of smooth muscle cells, elastic fibers, and connective tissue. The adventitia is the outermost layer and is composed of connective tissue, nerves, and blood vessels. When plaque develops in the vessel wall, the structure and composition of the vessel wall can change, resulting in thickening or hardening of the intima or media layer. This can narrow the lumen and reduce blood flow, potentially leading to a heart attack or stroke.

In healthy arteries, the layers of the IVUS image show a uniform thickness and a smooth luminal border. However, in the case of atherosclerosis, plaque accumulation can cause the layers to become uneven and the lumen to become irregularly shaped. This can result in reduced blood flow and an increased risk

of cardiovascular events.

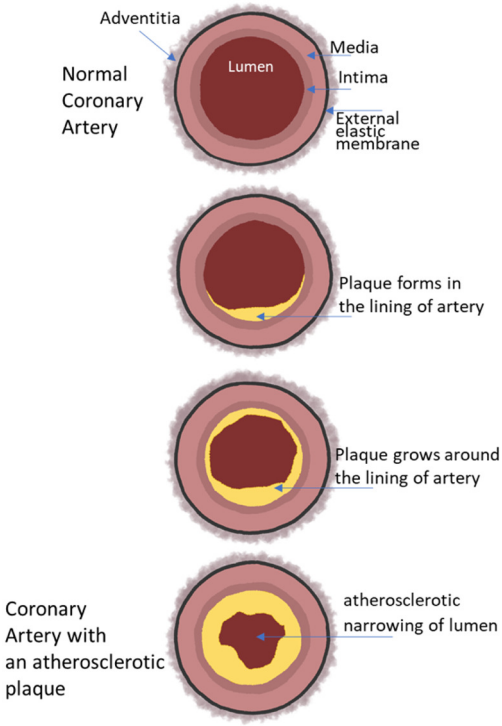

Fig.3: *Components of IVUS Images and the Effects of Plaque.*

B. Concentration of Entropy

Entropy provides a measure of the amount of information or uncertainty present in an image. It is calculated using the histogram of an image, which represents the distribution of pixel intensities. The entropy equation is given as

$$H = -\sum(p_i \log_2(p_i)) \tag{1}$$

Where H represents the entropy value, p_i is the probability of occurrence of each intensity value i, and the summation is performed over all possible intensity values. A high entropy value indicates that the pixel intensities are evenly distributed across the image, resulting in a more complex and information-rich image. Conversely, a low entropy value suggests that the pixel intensities are concentrated in a few regions, resulting in a simpler and less informative image.

C. Gradient Magnitude

Gradient magnitude (GM) is a measure of the strength or intensity of the gradient of an image. In image processing, the gradient refers to the change in intensity or color values between adjacent pixels in an image. The gradient magnitude is computed by taking the magnitude of the gradient vector, which is a two-dimensional vector that represents the direction and magnitude of the change in intensity between two adjacent pixels.

Mathematically, it can be represented as:

$$GM = \sqrt{(Gx)^2 + (Gy)^2} \tag{2}$$

$$Gx = \frac{\partial I(x,y)}{\partial x} \approx \frac{I(x+1,y) - I(x-1,y)}{2} \tag{3}$$

$$Gy = \frac{\partial I(x,y)}{\partial y} \approx \frac{I(x,y+1) - I(x,y-1)}{2} \tag{4}$$

Here, Gx and Gy represent the gradient values in the x and y directions, respectively.

The gradient magnitude is a useful feature in image processing tasks such as edge detection and image segmentation. In edge detection, the gradient magnitude is used to identify regions in the image where the intensity changes sharply, which corresponds to edges or boundaries between different objects or regions. In image segmentation, the gradient magnitude can be used to identify regions with similar texture or color by clustering pixels based on their gradient magnitudes.

D. Proposed Methods

Diagram of the proposed method for detecting plaque territory in the IVUS Images presented in Figure 4. The Methodology section should take into account the observed characteristics of Intravascular Ultrasound (IVUS) images, as previously mentioned. These images consist of four main components: the lumen, intima, media, and adventitia, which vary in size, texture, contrast, and brightness. IVUS images are typically low in brightness, and the lumen is situated within the media. Additionally, the lumen and media have low and high gradients, respectively. Plaque is located within the media area and has a non-geometric shape. The proposed framework for identifying plaque territory is classified into five steps: 1) Image Normalization, 2) Image Enhancement & Blob Analysis, 3) Media Boundary Estimation, 4) Random Spiral Walk, and 5) Identifying Plaque location & Estimating Plaque size, respectively.

D.1 Image Normalization

To reduce the variation in light intensity values within the image used in the experiment, image normalization is performed using the equation:

$$O(x,y) = \left(\frac{I(x,y) - \min(I)}{\max(I) - \min(I)}\right) \times (o_{\max} - o_{\min}) + o_{\min} \tag{5}$$

where: $O(x,y)$ is the normalized output pixel value at position (x,y). $I(x,y)$ is the original input pixel value at the same position. $\min(I)$ is the minimum

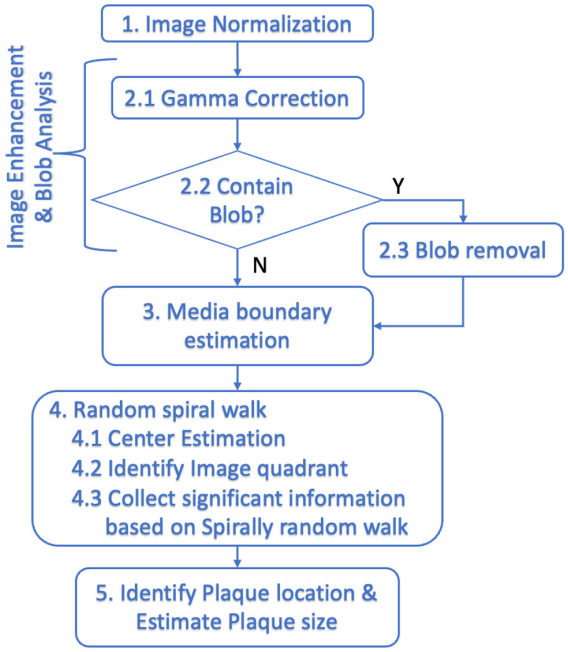

Fig.4: *Flow diagram of our proposed framework.*

pixel value in the original image. $\max(I)$ is the maximum pixel value in the original image. $o_{\min}$ is the minimum value of the desired output range. $o_{\max}$ is the maximum value of the desired output range.

By applying eq. (5) to each pixel in the image, the intensity values are normalized to the desired range, enabling better visualization or further processing of the image. Then the normalized image is used to identify the component using gamma correction approach.

D.2 Gamma Correction

The power gamma equation is a mathematical representation of the gamma correction technique used in image processing. It is defined as follows:

$$I_{out}(x,y) = \left(\frac{I_{in}(x,y)}{I_{max}}\right)^{\gamma} \tag{6}$$

where:

$I_{in}(x,y)$ is the input image pixel intensity at location (x,y).

I_{max} is the maximum pixel intensity value in the input image.

γ is the gamma value specified for gamma correction.

$I_{out}(x,y)$ is the output pixel intensity value after gamma correction.

Gamma correction is a technique used to adjust the brightness levels of an image by applying a nonlinear transformation to its pixel values. This technique uses a gamma value as an exponent to adjust the brightness levels of the image.

In the eq. (6), the input pixel intensity value $I_{in}(x,y)$ is normalized by dividing it by the maximum pixel intensity value I_{max}. This ensures that the pixel values are within the range of [0,1]. The gamma value γ is then applied as an exponent to this normalized pixel value, resulting in the output pixel intensity value $I_{out}(x,y)$.

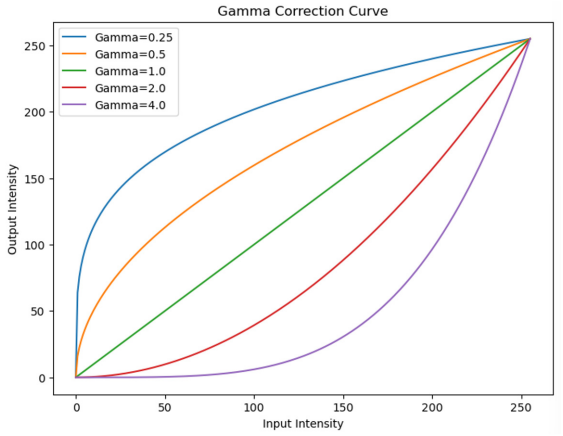

Fig.5: *Gamma Correction Curve.*

Figure 5 demonstrates the relationship between input and output intensity after gamma correction. Increasing the gamma value leads to a flatter curve, indicating darker images, while decreasing the gamma value creates a steeper curve, resulting in brighter images. Gamma correction is beneficial for enhancing contrast and brightness in low-contrast IVUS images. It addresses the uneven brightness increase across different areas, facilitating the delineation of media boundaries.

To accurately identify the media-adventitia boundary, we utilize gamma correction to enhance image clarity. We set the gamma value to 4.0 based on extensive observations, which helps determine the maximum radius for detecting potential plaque territory or Region of Interest (ROI).

Figure 6 presents the original IVUS image and the enhanced version with a gamma value of 4.0. The media boundary is clearly emphasized, enabling accurate differentiation from the adventitia.

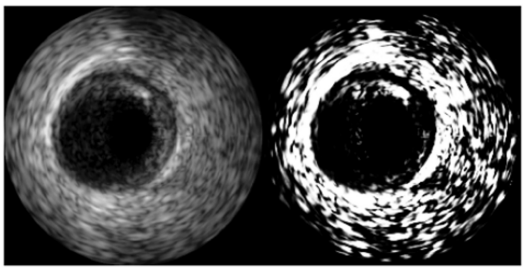

Fig.6: *Comparison of Original and Enhanced IVUS Images with Gamma correction at 4.0.*

The output from gamma correction step still has some blob inside Lumen and Media area. The noise and blob processing are accounted in the following steps.

D.3 Blob Analysis

- Noise reduction

The Walsh-Hadamard transform is applied as a low-pass filter to reduce high-frequency noise. The Hadamard unitary matrix of order n is an $N \times N$ matrix, $N = 2n$, defined by the recursive formula:
$H_n = H_1 H_n - 1$ where

$$H_1 = \frac{1}{\sqrt{2}} \begin{bmatrix} 1 & 1 \\ 1 & -1 \end{bmatrix} \tag{7}$$

Eq. (7) represents the Kronecker product. After the transformation, the filtered image demonstrates improved clarity, enabling a distinct differentiation between the Adventitia and Media layers.

- Blob Analysis

While the application of Gamma correction in Section D.2 contributes to reducing the intervening region between the media and lumen, performing blob analysis remains advantageous for achieving enhanced contour results. In this process, elimination of the occurred blob (Figure 2.D) can be achieved through the utilization of the region's properties [12] after Gamma correction enhancement. The scattered blob to be removed can be determined by utilizing the measurements of the major axis and minor axis.

In cases where small blobs, representing isolated connected areas, are encountered and labeled, they are removed before advancing to the subsequent analysis steps.

D.4 Media Boundary Estimation

In order to retrieve the media boundary, we first identified the circular-like shape in the middle of the image using contouring techniques, as shown in Figure 7. We then applied morphological operations, specifically erosion and dilation, to refine and enhance the boundary of the media. The erosion operation helps to shrink the boundary, while the dilation operation expands it.

After acquiring the contour boundary, we will be sampling the points within the area using the Spiral Walk approach.

D.5 Random Spiral Walk

- Center Estimation

To identify the maximum diameter and its midpoint in an asymmetrical circular shape, we follow these three steps:

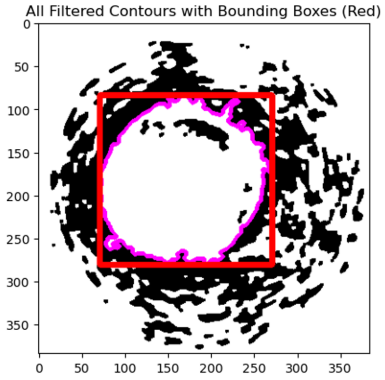

Fig.7: *Contoured object (media).*

→***step* 1:** Calculate the distances ($dist_i$) and angles (θ) for each point relative to the centroid by using the following formulas:

Let (x_i, y_i) represent the coordinates of each point i. The centroid is calculated using eq. (8) and (9) as the average of all point coordinates:

$$centroid_x = \frac{1}{N} sum(x_i) \tag{8}$$

$$centroid_y = \frac{1}{N} sum(y_i) \tag{9}$$

where N is the total number of points. Calculate the distances ($dist_i$) from each point to the centroid using eq. (10).

$$dist_i = \sqrt{(x_i - centroid_x)^2 + (y_i - centroid_y)^2} \tag{10}$$

Calculate the angles (θ) for each point relative to the centroid using eq. (11):

$$\theta_i = \arctan^2(y_i - centroid_y, x_i - centroid_x) \tag{11}$$

→***step* 2:** step2: Identify the combination with the longest total length. For each point i, calculate the sum of the distances between the point at angle θ_i and the centroid, and also the point at angle $(-180 + \theta_i)$ and the centroid using eq. (12):

$$total\_length_i = dist_i + dist_j \tag{12}$$

where j is the index corresponding to (-180+θ_i).

→***step* 3:** Identify the combination (i, j) using eq. (13), and (14) with the longest $total\_length_i$

$$midpoint_x = \frac{x_i + x_j}{2} \tag{13}$$

$$midpoint_y = \frac{y_i + y_j}{2} \tag{14}$$

where (x_i, y_i) and (x_j, y_j) are the coordinates of the two points that form the maximum diameter.

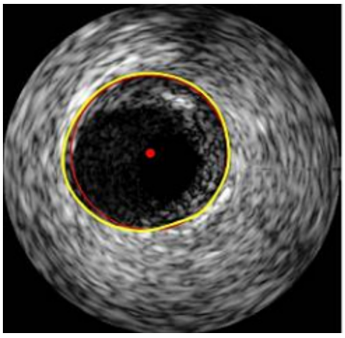

Fig.8: *The result of center estimation.*

Figure 8 provides a visual representation of the midpoint. The midpoint is of crucial importance as it serves as the central point to initiate the subsequent spiral walk. This deliberate choice ensures that the spiral trajectory covers the entire area of the media comprehensively. By utilizing the midpoint as the starting position, the media can be thoroughly explored, enabling a comprehensive examination of the underlying content.

- Random Spiral Walk

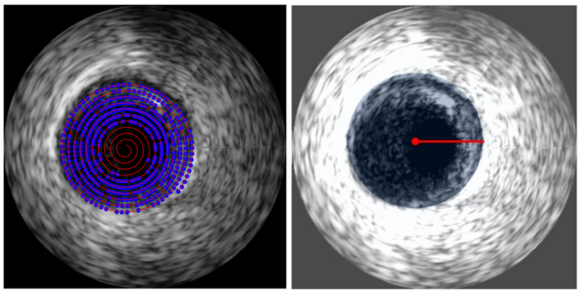

Fig.9: *Random Indices on Random Spiral Walk.*

To identify plaque territory, we propose a random spiral walker algorithm that generates a spiral trajectory within a defined region. The algorithm is initialized with a seed point (x_0, y_0) and iteratively extends the trajectory as shown in figure 9, using the eq. (15), and (16). Polar to Cartesian conversion:

$$x = r * \cos(\theta) \tag{15}$$

$$y = r * \sin(\theta) \tag{16}$$

Update of polar coordinates:

$$r = r + step_{size} \tag{17}$$

$$\theta = \theta + angle_{increment} \tag{18}$$

The algorithm continues this process until a termination condition is met, typically based on the distance from the starting point exceeding a predefined threshold.

In our study, we enhance the analysis by introducing a Markov chain-based approach for generating random indices. This approach can be framed within the context of a Probabilistic Model, where we consider the transition matrix, P, as the probability distribution function.

The transition matrix, denoted as $P(i, j)$, represents the probability of transitioning from point i to point j in the trajectory. This can be expressed mathematically as

$$P(i, j) = P(X = j | X = i) \tag{19}$$

where $P(X = j|X = i)$ denotes the probability of transitioning from point i to point j.

To construct the transition matrix P, we consider specific criteria and considerations relevant to our application. Factors such as the relative positions of points, the local structure of the object, and the desired characteristics of the random walk are taken into account when assigning probabilities to the transitions between points.

During the random walk, at each step, the walker selects the next point based on the probabilities defined by the transition matrix P. This can be represented mathematically as:

$$X(t + 1) = j, \ where \ j \ \sim \ P(X = j | X = i) \tag{20}$$

where $X(t+1)$ represents the state or point at time $t+1$, and j is sampled from the probability distribution defined by the transition matrix P.

By utilizing this Markov chain-based approach within the framework of a Probabilistic Model, we can select random indices that provide additional insights into the object's characteristics, such as the gradient magnitude and entropy. These random indices serve as samples from the underlying probability distribution defined by the transition matrix, enabling us to explore different points within the region of interest (ROI) and gain a deeper understanding of the underlying object.

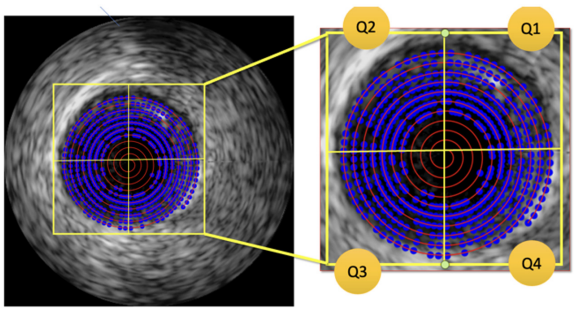

Fig.10: *ROI quadrant separation.*

Figure 10 demonstrates that ROI is divided into four quadrants, labeled Q1, Q2, Q3, and Q4 accordingly. Each quadrant provides a coarse estimate of the plaque's size.

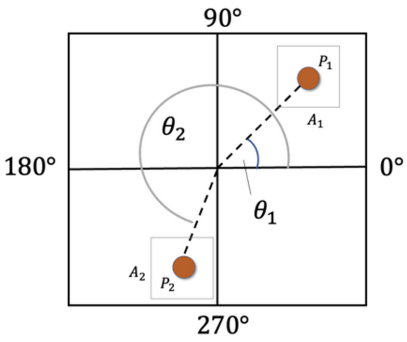

Fig.11: *Demonstration of random point in each quadrant.*

Figure 11 shows the demonstration of the random point P1 has an angle (θ_1) between 0 and 90 degrees; it is in the Q1. More than 90 but fewer than 180 are contained in Q2. More than 180 but less than 270, it falls into the third quarter. It is greater than 270 in Q4.

The square area surrounding each random point $(A1, A2, \ldots, An)$ is then used to determine the area within ROI.

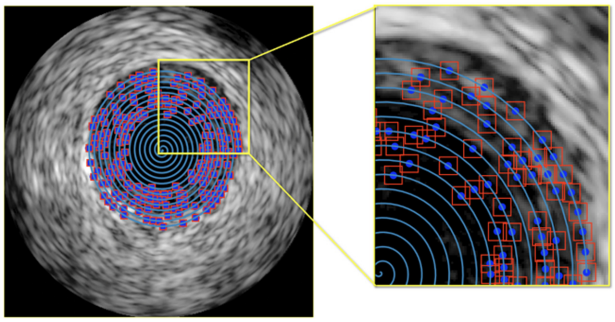

Fig.12: *Area of 8×8 around the random point.*

Through our observation, we have noticed that regions corresponding to the lumen tend to exhibit significantly lower gradient values compared to areas occupied by plaque, as illustrated in Figure 12. Leveraging this characteristic, we can employ a Markov chain-based approach using random indices to estimate potential plaque regions within the defined ROI. By selecting indices associated with gradient magnitudes higher than 2.0 times the standard deviation or approximately 5% of the values, we can identify regions that are more likely to represent plaque areas. Figure 13. illustrates the density graph of the gradient magnitude within the ROI. This methodology enhances the accuracy and effectiveness of our analysis in identifying and characterizing plaque territories within the ROI.

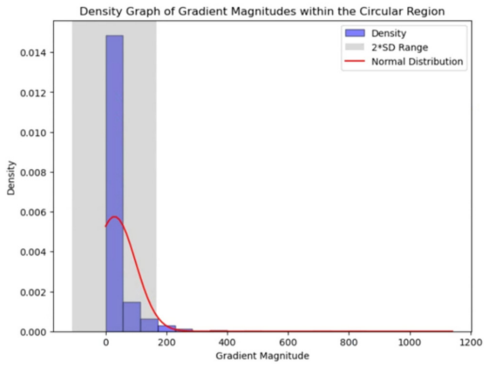

Fig.13: *Density of gradient magnitude in the random area.*

In addition, based on the observation, the lumen region tends to be more stable. Therefore, the entropy value is used to determine the location of plaques in each quadrant. In Figure 14, the entropy is calculated using the rectangle's area $(A1, A2, \ldots, An)$. Areas with a lower entropy are depicted by smaller circles. The area represented by the larger circle has a greater entropy.

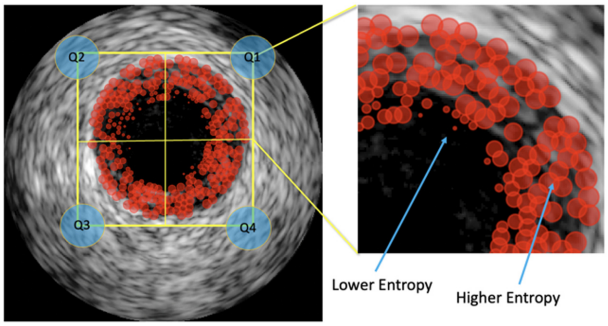

Fig.14: *Bubble plot of concentration of entropy in each area.*

Then, the regions with the lowest entropy are eliminated, as shown in Figure 15. To determine the plaque area, every intended region with a higher entropy value is maintained.

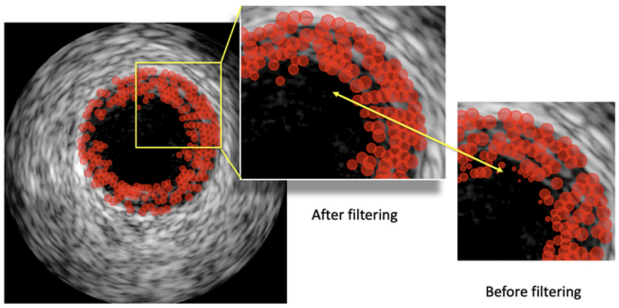

Fig.15: *The result of entropy filtering process.*

The calculated entropy is then summed in each quadrant of ROI. The area with the highest sum of entropy value is the target for plaque occurrence.

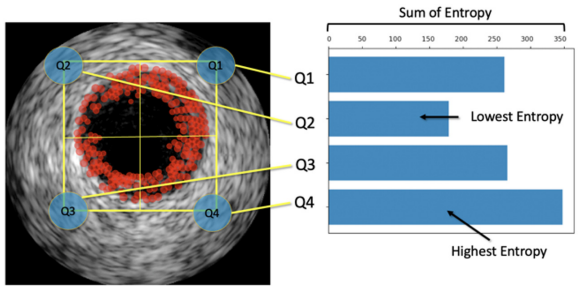

Fig.16: *the entropy concentration level of each quadrant.*

Figure 16 depicts the consequence of adding the values of entropy in each quadrant. In this instance, the quadrant with the greatest entropy value is quadrant 4 (Q4). It means that clinicians can concentrate on the Q4 region. In contrast, the Q2 region has the lowest entropy. Then, we can disregard the area to reduce computational effort in subsequent considerations. The plaque territory identification can be described in the following algorithm.

Algorithm: Plaque territory identification
Input: Set of random points S
Begin
Foreach processor $P_j(S)$, $j \leq 4$
1 **For** i ← 0 **to** number of sets n_s
2 **Compute** area A_i around the point S_i
3 **Compute** entropy E_i and gradient G_i of area A_i
4 **If** E_i and G_i reach threshold, T **then**
5 **Determine** the plaque area K_i
6 **End If**
7 **End for**
End
Output: Set of plaque area from each processor $K_{p_1}, K_{p_2}, K_{p_3}, K_{p_4}$

The result from the proposed approach will be discussed in the next section.

4. EXPERIMENTAL RESULT AND DISCUSSION

A. Dataset

To substantiate the proposed methodology, we employ a set of 203 Intravascular Ultrasound (IVUS) dataset that is openly accessible to the wider population [5]. This specific investigation solely examined dataset B. The resolution of the system is 384 × 384 pixels, while the ultrasonic frequencies utilized range up to 20 MHz. For the purpose of this study, we exclusively utilize the training data acquired from dataset B. This study employs a framework, as shown in Figure 4 to accurately ascertain the area of plaques in the given images.

The dataset is at full pullback 3D context multi-frame datasets. The end-diastolic cardiac pullback yields 20–50 gated frames. Each frame has four DICOM pictures.

The pullback volumetric analysis dataset has enough frames. The cardiac contraction swings IVUS pullbacks. The catheter oscillates transversely (axially, back and forth the vessel) due to this artefact, resulting in numerous vascular position samples. Extracting pullback frames from a specific cardiac phase (using ECG or image-based gating) yields a coherent spatial scan of the vessel's shape in 3D. Any other pullback frame corresponds to a different cardiac phase, therefore the artery diameter may have expanded and the IVUS frame's position along the vascular morphology is unclear. The swinging causes the IVUS frame that spatially proceeds to be the previous gated frame. Given this, a volumetric pullback evaluation should only use gated frames (manually labelled frames).

Table 1: *Window size selection using its accuracy.*

Window Size	Accuracy	Precision	Recall
3×3 px	0.58	0.57	0.57
4×4 px	0.65	0.67	0.66
6×6 px	0.79	0.71	0.74
8×8 px	**0.8**	**0.81**	**0.81**
10×10 px	0.81	0.8	0.83
12×12 px	0.85	0.85	0.83
14×14 px	0.82	0.85	0.85

The previous and succeeding gated frames, not the neighboring frames, offer spatial context for segmentation. However, certain algorithms may need frames that are temporally nearby in the pullback acquisition to use the blood scatterer de-correlation for lumen segmentation. For this reason, five chronologically neighboring frames (two before and two after) have been included. More than two frames ahead (and backward) in time may not align consecutive IVUS frames. IVUS pullbacks include rotating artefacts, and the vessel may start pulsing, changing its diameter. These two occurrences prevented algorithms from exploiting frame correlation.

B. Performance Evaluation Metrics

To assess the performance of the proposed plaque localization method, several evaluation metrics are computed, including accuracy, precision, recall, and F1-score. These metrics provide quantitative measures of the method's ability to detect and localize plaque regions in IVUS images accurately.

The utilization of the confusion matrix is prevalent in the assessment of performance for diverse machine learning endeavors, encompassing picture segmentation. The nature of the image segmentation problem makes it particularly relevant for evaluation purposes.

The confusion matrix is an adaptable evaluation tool that offers useful insights into the performance of picture segmentation models. The utilization of this approach facilitates a thorough examination of the model's merits and drawbacks, hence assisting in the identification of areas for development to optimise the segmentation task's overall efficacy.

In the evaluation of entropy concentration, the 8x8 pixel region surrounding the random point is chosen,

Table 2: *Performance of the proposed method using confusion matrix.*

	Accuracy	*Precision*	*Recall*	*F1-Score*
Entropy Method Gradient Magnitude Method	0.71	0.81	0.69	0.91
Proposed Method (Entropy+ Gradient Magnitude)	0.78	0.72	0.62	0.69
	0.89	0.81	0.77	0.83

as illustrated in Figure 17. The precision comparison for each size is presented in Table 1. Additionally, the performance of the proposed method using a confusion matrix is displayed in Table 2.

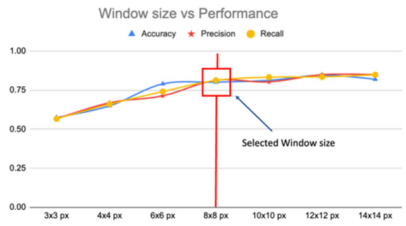

Fig.17: *area size selection graph.*

Moreover, U-net architecture is employed to compare the features with 10-fold validation. For classifying IVUS images, the U-Net architecture works as follows: The contracting path uses convolutional layers with down-sampling operations (e.g., max-pooling) to capture relevant features at multiple scales. This enables the model to grasp both local and global context information from the IVUS images, crucial for accurate classification. Subsequently, the expanding path employs convolutional layers with up-sampling operations (e.g., transposed convolutions) to generate a segmentation mask highlighting regions of interest in the IVUS image.

In summary, neither traditional image classification methods nor deep learning methods are categorically better than the other. Traditional methods can be useful in specific contexts, especially when dealing with smaller datasets, limited computational resources, or when interpretability is critical. On the other hand, deep learning excels in large-scale image classification tasks, where automatic feature learning and scalability are significant advantages. The choice of method depends on the task requirements, data availability, and computational resources.

C. Quantitative Results

The proposed method is evaluated on the test set comprising a diverse range of IVUS images. The results in Table 2. demonstrate the effectiveness of the method in accurately identifying and localizing plaque regions. The quantitative results obtained are as follows:

Accuracy: The accuracy metric measures the overall correctness of the method in correctly classifying plaque and non-plaque regions. The proposed method achieves an accuracy of 0.89, indicating its high level of accuracy in distinguishing between plaque and non-plaque areas.

Precision: Precision quantifies the proportion of correctly detected plaque regions among all the regions classified as plaques. The proposed method achieves a precision score of 0.81, indicating that the majority of regions identified as plaques are indeed true positive detections.

Recall: Recall, also known as sensitivity, measures the ability of the method to identify all the true positive plaque regions. The proposed method achieves a recall of 0.77, indicating its effectiveness in capturing a substantial portion of the true positive plaques present in the images.

F1-score: The F1-score is the harmonic mean of precision and recall, providing an overall measure of the method's performance. The proposed method achieves an F1-score of 0.83, indicating a well-balanced trade-off between precision and recall.

D. Qualitative Results

In addition to the quantitative evaluation, a qualitative assessment of the proposed method is performed by visually inspecting the localized plaque regions in the IVUS images. A set of representative images from the test set are selected, and the plaques identified by the proposed method are overlaid on the original images.

The qualitative analysis demonstrates the method's ability to accurately delineate the boundaries of plaque regions, providing a clear visualization of the areas affected by atherosclerosis. The localized plaques align well with the annotations made by expert cardiologists, confirming the method's accuracy in identifying and localizing plaque regions within the arterial walls.

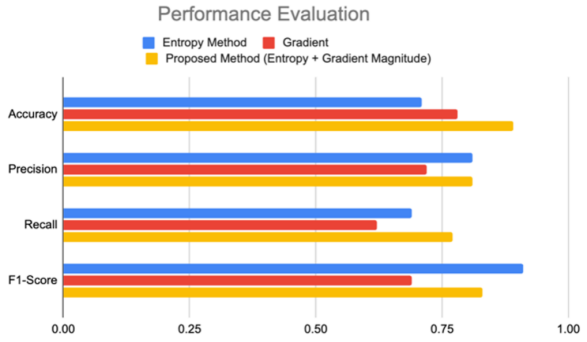

Fig.18: *Performance Evaluation Result.*

The comparative analysis reveals in Figure 18 that the proposed method outperforms the existing methods in terms of accuracy, precision, recall, and F1-

score. The proposed method consistently achieves higher scores across all evaluation metrics, indicating its superiority in accurately detecting and localizing plaque regions in IVUS images. Moreover, the proposed method demonstrates robustness and generalization capabilities across various IVUS image datasets.

E. Computational Efficiency

The computational efficiency of the proposed method is also evaluated to assess its feasibility for real-time clinical applications. The experiments are conducted on a standard workstation with an Apple M1 processor and 8GB of RAM.

The proposed method demonstrates efficient performance, with an average processing time of 0.2 seconds per IVUS image. The real-time processing capabilities make it suitable for integration into clinical workflows, facilitating quick and reliable plaque localization during diagnosis and treatment planning.

F. Comparison with Existing Methods

To further validate the effectiveness of the proposed method, a comparative analysis is conducted with existing plaque localization methods reported in the literature. Several state-of-the-art techniques, including method Faraji et. al., J. Onpans et. al., L. Verico et. al., and Ecarchos et. al., are selected for comparison. The performance comparison results can be presented in Table 3.

Table 3: *Performance comparison of the proposed approach and other recent methods.*

	Media		***Lumen***	
Method	***HD***	***JM***	***HD***	***JM***
Faraji *et al.*[6]	0.67	0.77	0.30	0.87
J. Onpans *et al.*[4]	-	-	0.10	0.82
L. Verico *et al.*[8]	0.57	0.83	0.32	0.88
Exarchos *et al.*[5]	0.60	0.79	0.42	0.81
Proposed	0.51	0.88	0.31	0.89

In Table 3, we have the average performance scores for estimating the media and lumen regions using two evaluation metrics: Hausdorff (HD) and Jaccard (JM). The comparative results show that, for the Lumen, [4] achieves the lowest HD scores, outperforming our proposed method. However, when it comes to JM, our proposed method demonstrates greater reliability compared to alternative methods, whether we're estimating the media and lumen or not. Moreover, when estimating the media region, our proposed method performs exceptionally well, whether it's in terms of HD or JM.

5. DISCUSSION

From the experimental results, it is evident that our proposed method performs well compared to other benchmarks, as shown in Table 3. Additionally, our method can efficiently scan and detect plaque regions quantitatively, allowing us to separate them according to quadrants.

However, our proposed method does have limitations. Firstly, a constraint of this research emerges in scenarios where the light intensity disparity between the adventitia and the media is identical. This circumstance can lead to an inability to precisely segment the media from the adventitia, potentially causing errors in subsequent workflow stages. Moreover, the precision of center estimation might be influenced by the presence of artifacts along the boundary of the media section, such as shadows, blurriness, and similar issues. Additionally, the enhancement technique, which involves gamma value adjustments based on observations, experimentation, and trial and error, might have alternative avenues for improvement. An adaptive approach, for instance, could potentially yield more substantial enhancements in experimental outcomes.

6. CONCLUSIONS

This paper presents a simple and optimal approach to classify plaque territories in IVUS images. Unlike existing techniques that rely on circular algorithms, our method focuses on enhancing the brightness of the adventitia, which is the largest part of the image. This enhancement aids in detecting other components. We address the challenge of low contrast in IVUS images, which often results in unclear edges, by proposing the use of Gamma Correction and blob analysis techniques. By accurately calculating the boundary of the media and identifying the region of interest (ROI), we can determine the size and position of the plaque territory. Overall, this paper tackles the research problem by incorporating image enhancement, boundary calculation, and plaque measurement. In future work, beyond using Gradient Magnitude and Entropy as features, there may be other characteristics that prove more effective in revealing concealed information, thus further addressing our challenge.

ACKNOWLEDGMENT

The authors gratefully acknowledge the financial support from the Faculty of Informatics at Burapha University. Special thanks to Dr. Watcharaphong Yookwan for his valuable insights and contributions to this research. The authors also acknowledge the assistance of the Institutional Review Board of Burapha University with reference number HS040/2566.

References

[1] J. Yang, L. Tong, M. Faraji and A. Basu, "IVUS-Net: An Intravascular Ultrasound Segmentation Network," *International Conference of Smart Multimedia*, vol. 11010, pp. 367-377, June 2018.

[2] J. Lee, Y. N. Hwang, G. Y. Kim, J. Yean Kwon and S. M. Kim, "Automated classification of dense calcium tissues in gray-scale intravascular ultrasound images using a deep belief network," *BMC Medical Imaging*, vol. 19, no. 103, 2019.

[3] L. L. Vercio, M. d. Fresno and I. Larrabide, "Lumen-intima and media-adventitia segmentation in IVUS images using supervised classifications of arterial layers and morphological structures," *Computer Methods and Programs in Biomed*, vol. 177, pp. 113-121, 2019.

[4] J. Onpans, W. Yookwan, J. Sangrueng and S. Srikamdee, "Intravascular Ultrasound Image Composite Segmentation using Ensemble Gabor-spatial Features," *2022 13th International Conference on Information and Communication Technology Convergence (ICTC)*, Jeju Island, Korea, pp. 1499-1504, 2022.

[5] S. Baloccoet *al.*, "Standardized evaluation methodology and reference database for evaluating IVUS image segmentation," *Computerized medical imaging and graphics*, vol. 38, no. 2, pp. 70-90, 2013.

[6] X. Li *et al.*, "Coronary Plaque Classification of Intravascular Ultrasound Images based on a Multi-Stage Deep Classifier Cascades," *2022 IEEE International Ultrasonics Symposium (IUS)*, Venice, Italy, pp. 1-3, 2022.

[7] M. Faraji, I. Cheng, I. Naudin and A. Basu, "Segmentation of arterial walls in in- travascular ultrasound cross-sectional images using extremal region selection," *Ultrasonics*, vol. 84, pp. 356–365, 2018.

[8] L. L. Vercio, M. Del Fresno and I. Larrabide, "Lumen-intima and media-adventitia segmentation in IVUS images using supervised classifications of arterial layers and morphological structures," *Computer Methods and Programs in Biomedicine*, vol. 177, pp. 113-121, 2019.

[9] H. Shinohara *et al.*, "Automatic detection of vessel structure by deep learning using intravascular ultrasound images of the coronary arteries," *Plos One*, vol. 16, pp. 1–14, 2021.

[10] Fubao Zhu *et al.*, "A Deep Learning-based Method to Extract Lumen and Media-Adventitia in Intravascular Ultrasound Images," *Ultrason Imaging*, vol. 44, no. 5-6, pp. 191-203, 2022.

[11] J.-E. Park *et al.*, "TCTAP A-044 Deep Learning Segmentation of Lumen and Vessel on IVUS Images," *Journal of the American College of Cardiology*, vol. 77 , no.14, 2021.

[12] W. Yookwan, K. Chinnasarn and B. Jantarakongkul, "Automated Vertebrae Pose Estimation in Low-Radiation Image using Modified Gabor Filter and Ellipse Analysis," *2018 5th International Conference on Advanced Informatics: Concept Theory and Applications (ICAICTA)*, Krabi, Thailand, pp. 141-146, 2018.

Benchaporn Jantarakongkul attained her B.Sc. in Applied Mathematics and M.Sc. in Information Technology degrees from King's Mongkut Institute of Technology, Ladkrabang in 1996 and 1998, sequentially. During the period spanning 1998 to 2006, she assumed the role of lecturer in the Department of Computer Science at Burapha University, Chonburi, Thailand. Commencing in 2007, she has held the position of lecturer in the Faculty of Informatics at Burapha University, Thailand. Her areas of research interest include Management Information System, Human Computer Interaction, Accessibility, Usability, Automation, Computer System, Machine Learning and Digital Image Processing.

Pusit Kulkasem obtained his B.Eng. (Electronics and Information Sciences) and M.Eng. (Master of Engineering) degrees from the University of Tsukuba, Japan, in 1997 and 1999, respectively. From 1999 to 2006, he served as a lecturer in the Department of Computer Science at Burapha University, Chonburi, Thailand. Since 2007, he has held the position of lecturer within the Faculty of Informatics at Burapha University, Thailand. His research interests encompass Computer Networks, Machine Learning, and Digital Image Processing.